RESEARCH ARTICLE

Pan-cancer analysis of USP2 and its prognostic value in kidney renal clear cell carcinoma along with related immune function analysis

Bowen Yan[1], Yanan Zhang[2], Jinhai Huo[2, *], Weiming Wang[1, 2, *]

[1]College of Pharmacy, Heilongjiang University of Chinese Medicine, Harbin, Heilongjiang, China. [2]Chinese Medicine Research Institute, Heilongjiang Academy of Chinese Medical Sciences, Harbin, Heilongjiang, China.

Received: December 16, 2024; **accepted:** April 1, 2025.

Ubiquitin-specific peptidase 2 (USP2) is a crucial deubiquitylating enzyme (DUB) belonging to the peptidase C19 superfamily. Despite emerging evidence of DUBs' involvement in tumor progression, USP2's pan-cancer expression patterns and its mechanistic contributions to kidney renal clear cell carcinoma (KIRC) pathogenesis remain unexplored. This study investigated pan-cancer expression profiling through integrated analysis of TCGA, GTEx, and CCLE datasets. DNA methylation patterns in KIRC were characterized using MethSurv platform. Immune microenvironment interactions were decoded through multi-algorithmic approaches (CIBERSORT, EPIC, TIMER). Single-cell resolution mapping was performed *via* TISCH2. Identify characteristic genes in KIRC using machine learning. Functional networks were constructed using STRING with GSEA validation. The results showed that USP2 demonstrated significant differential expression in KIRC compared to normal renal tissues with its downregulation exhibiting strong prognostic relevance to advanced tumor staging (T3 - T4) and diminished survival outcomes. Mechanistically, USP2 appeared to exert tumor-suppressive functions through immune microenvironment modulation as evidenced by its correlation with antitumor immune signatures and checkpoint regulators. The consistent association between USP2 hypermethylation at promoter CpG sites and transcriptional silencing suggested epigenetic regulation of this pathway. These results positioned USP2 as a promising immunotherapeutic biomarker candidate in KIRC, warranting further validation through prospective clinical cohorts and functional mechanistic investigations.

Keywords: pan-cancer; bioinformatics analysis; USP2; clear cell renal cell carcinoma; immunity; machine learning; single-cell transcriptome sequencing.

[*]**Corresponding authors:** Jinhai Huo, Chinese Medicine Research Institute, Heilongjiang Academy of Chinese Medical Sciences, Harbin 150036, Heilongjiang, China. Weiming Wang, College of Pharmacy, Heilongjiang University of Chinese Medicine, Harbin 150040, Heilongjiang, China; Chinese Medicine Research Institute, Heilongjiang Academy of Chinese Medical Sciences, Harbin 150036, Heilongjiang, China. Emails: jinhaihuo@126.com (Huo J), zyyjy@163.com (Wang W).

Introduction

Renal cell carcinoma (RCC), a highly aggressive malignancy of the urinary system, accounts for 2 - 3% of adult cancers and ranks third in urologic malignancies after prostate and bladder cancers [1, 2]. Clear cell RCC (ccRCC), representing 75 - 80% of RCC cases, demonstrates pronounced tumor heterogeneity, frequent metastasis, and dismal prognosis with a 5-year survival rate below 10% for advanced-stage patients [3-5]. Current therapeutic strategies including targeted therapies and immunotherapies yield limited clinical benefits due to intrinsic resistance mechanisms [6].

The ubiquitin-proteasome system (UPS), a critical post-translational regulatory axis, governs protein homeostasis through balanced ubiquitination and deubiquitination [7, 8]. Dysregulation of UPS components drives carcinogenesis by stabilizing oncoproteins such as NF-κB or degrading tumor suppressors like p53 [9-11]. Ubiquitin-specific protease 2 (USP2), a member of the deubiquitinating enzyme family, modulates key cancer pathways by regulating protein stability [12]. Emerging evidence highlights its dual roles in tumorigenesis, which includes that USP2 stabilizes TRAF2 to enhance inflammatory signaling [13], while paradoxically promotes PD-L1 degradation to impair antitumor immunity [14]. Mechanistically, USP2 orchestrates immune regulation *via* the VPRBP-p53 axis [11] and facilitates tissue repair in inflammatory diseases [15]. Despite these advances, critical knowledge gaps persist. First, USP2's pan-cancer expression patterns remain unmapped, limiting the understanding of its tissue-specific oncogenic effects. Second, in ccRCC context, USP2's functional crosstalk with epigenetic regulators and tumor microenvironment components is completely unexplored. Third, existing studies predominantly focus on gastrointestinal and pulmonary malignancies [16, 17], leaving renal cancer biology conspicuously underinvestigated.

This study systematically investigated USP2's oncogenic roles through two complementary approaches of pan-cancer analysis of USP2 expression, epigenetic regulation, and prognostic significance across 34 malignancies and dissection of USP2-mediated immune modulation in ccRCC using TCGA/GEO cohorts and single-cell transcriptomics. The bulk RNA-seq (TCGA, GTEx), DNA methylation arrays (MethSurv), and immune infiltration algorithms (CIBERSORT, TIMER) were integrated to map USP2's molecular landscape. Functional enrichment analysis (GSEA) and protein interaction networks (STRING) were employed to elucidate pathway associations, while scRNA-seq (TISCH2) resolved cell-type-specific expression patterns. By establishing USP2 as a novel immunomodulatory hub in ccRCC, this work provided a rationale for targeting USP2-mediated deubiquitination to overcome therapy resistance. The identified crosstalk between USP2 and PD-L1 pathways would offer actionable insights for developing combination immunotherapies.

Materials and methods

Data mining and processing

The standardized pan-cancer datasets including The Cancer Genome Atlas (TCGA), Therapeutically Applicable Research to Generate Effective Treatments (TARGET), and Genotype-Tissue Expression (GTEx), collectively abbreviated as PANCAN, were obtained from the UCSC Xena database (https://xenabrowser.net/). A total of 19,131 biological samples (N) of tumors specimen, normal tissues, or blood samples were included in the standardized pan-cancer dataset, while 60,499 genes or transcriptomic features (N) annotated by identifiers such as Ensembl IDs were measured across all samples. Expression data of USP2 (Ensemble ID. ENSG00000036672) were extracted from all samples with subsequent selection of specimen types including solid tissue normal, primary solid tumor, primary tumor, normal tissue, primary blood derived cancer - bone marrow, and primary blood derived cancer - peripheral blood. The term "each sample" referred to all individual biological specimens retained after stringent filtering of the original TCGA, TARGET, GTEx datasets. All expression values underwent $\log_2(x + 0.1)$ transformation followed by exclusion of cancer types containing fewer than three samples per category, yielding expression profiles for 34 distinct cancer types. Gene expression profiles from the Gene Expression Omnibus (GEO) (http://www.ncbi.nlm.nih.govgeo/) datasets (GSE781 and GSE53000, total n = 113) meeting the inclusion criterion (> 20 samples per dataset) were acquired. Batch effect correction was performed using the R 'sva' package with RNA-seq data processing executed through the 'limma' package. Machine learning algorithms

(LASSO and SVM) were employed for feature gene selection accompanied by construction of a protein-protein interaction network.

USP2 analysis of available cell lines in the Cancer Cell Line Encyclopedia (CCLE) database

Multi-omics data encompassing RNA-seq data, DNA methylation profiles, somatic mutation records, and copy number variation (CNV) data from human cancer cell lines were retrieved from Cancer Cell Line Encyclopedia (CCLE) database (https://portals.broadinstitute.org/CCLE). USP2 expression levels across distinct tissue types and malignant cell lineages were comparatively analyzed. Data visualization was executed using the ggplot2 package in R.

Analysis of genetic variation

Pan-cancer analysis of USP2 gene alterations was conducted through the cBioPortal platform (https://www.cbioportal.org). Tumor samples derived from TCGA database were analyzed, revealing inter-tumor variability in genetic alteration profiles across three parameters of alteration frequency, mutation type distribution, and copy number alteration (CNA) patterns.

USP2 DNA methylation analysis

USP2 methylation datasets were obtained simultaneously during pan-cancer USP2 transcriptome expression data acquisition from TCGA dataset. The data types included clinical data and corresponding TCGA dataset, RNA-seq data, and Methylation450K data. The methylation chips were annotated and a pan-cancer methylation analysis of USP2 was carried out. Furthermore, the Shiny Methylation Analysis Resource Tool (SMART) application (http://www.bioinfo-zs.com/smartapp/) and the MethSurv (https://biit.cs.ut.ee/methsurv/) databases were utilized to investigate the relationship between USP2 DNA methylation levels and gene expression, as well as the correlation between gene methylation degree and overall survival (OS) prognosis in kidney renal clear cell carcinoma (KIRC) patients.

Subsistence analysis

Analysis of USP2 expression trends across 34 cancer types identified malignancies demonstrating significant differential expression between tumor and adjacent normal tissues. RNA-seq data generated through the STAR alignment pipeline were standardized with subsequent extraction of TPM-formatted expression matrices and clinical annotations. Specimens lacking matched clinical metadata or representing normal tissue controls were excluded. Cox proportional hazards regression analysis was implemented using the survival package (v3.3-1) to assess prognostic associations [18].

Analysis of co-expressed genes and differentially expressed genes

Co-expression analysis of USP2 in KIRC was performed using the LinkedOmics database (http://www.linkedomics.org/login.php) with TCGA RNA-seq data. Pearson correlation coefficients were calculated through the platform's analytical module with co-expressed genes visualized in volcano plot format. The TCGA-KIRC cohort was stratified into USP2-low and USP2-high subgroups based on median expression thresholds. Differential expression analysis between subgroups was conducted using the limma package (v3.54.2, R4.2.1) with significantly differentially expressed genes (DEGs) identified at false discovery rate < 5%. Intersection analysis of DEGs and co-expressed genes was subsequently performed with results visualized through ggplot2 (v3.4.2) and VennDiagram (v1.7.3) packages.

Functional enrichment analysis

Functional enrichment analysis was implemented using the clusterProfiler package (R4.2.1) with z-score calculation for each enriched term performed through the GOplot package. Gene Ontology (GO) (http://geneontology.org/) annotation, Kyoto Encyclopedia of Genes and Genomes (KEGG) (https://www.genome.jp/kegg/) pathway analysis, and tissue-specific enrichment evaluation were systematically conducted on the identified intersecting gene set. Visualization of

analytical results was achieved using ggplot2 graphical parameters.

Gene set enrichment analysis

Gene Set Enrichment Analysis (GSEA) was performed using GSEA v4.1.0 (http://www.broadinstitute.org/gsea) on the intersecting gene set. The "c2.cp.v2022.1.Hs.gmt" gene set collection from MSigDB (https://www.gsea-msigdb.org/gsea/msigdb/collections.jsp) served as the reference database. Significant pathway enrichment was defined by the following thresholds as nominal *P* value < 0.05, false discovery rate (FDR) < 0.25, adjusted *P* value < 0.05, and normalized enrichment score (NES) absolute value > 2 [19].

Construction and visualization of the Protein-Protein Interaction network

Protein-protein interaction (PPI) network analysis was conducted using the STRING database (https://string-db.org/) with 357 intersecting genes. The Cytoscape platform (v3.9.1) was employed for network visualization with the MCODE plugin (v2.0.2) implementing cluster detection under defined parameters (node degree ≥ 2, k-core ≥ 5) to identify hub genes [20-22]. Machine learning algorithms (SVM and LASSO) were applied to process GSE781 and GSE53000 expression matrices from GEO (https://www.ncbi.nlm.nih.gov/geo/), enabling identification of disease-associated signature genes. A composite PPI network integrating USP2 with these characteristic genes was subsequently constructed.

Immune-related analysis

After downloaded and organized the pan-cancer dataset, the correlation between USP2 (ENSG00000036672) and the marker genes of five immune pathways as well as 60 dual-type immune checkpoint pathway genes were calculated [23, 24].

Immune infiltration analysis

Gene expression profiles across tumor types were extracted from the pan-cancer dataset and annotated with standardized GeneSymbol identifiers. Tumor-specific immune scores were calculated using the ESTIMATE package (v1.0.13) in R, enabling quantitative evaluation of tumor microenvironment characteristics [25]. Immune infiltration-USP2 correlations were systematically assessed through the psych package (v2.1.6) with pan-cancer relevance quantified by Pearson coefficients. Seven computational algorithms including TIMER, EPIC, IPS, MCPcounter, xCELL, CIBERSORT, QUANTISEQ were implemented to evaluate USP2-associated immune cell infiltration patterns. Correlation analysis encompassed both lymphoid and myeloid lineage populations across all TCGA tumor cohorts.

Single-cell sequencing

The CancerSEA database (http://biocc.hrbmu.edu.cn/CancerSEA/) was used to analyze the correlation of USP2 with the biological behavior of tumor cells in different tumors. Single cell datasets were obtained by using the TISCH2 tool (http://tisch.comp-genomics.org/home/) for cell type annotation, differential gene analysis and visualization.

Statistical analysis

SPSS 27.0 (IBM, Armonk, NY, USA) was employed with Python 3.9 supporting auxiliary data preprocessing through SciPy 1.7.1 for normality/variance checks of this research. For numerical variables between two-group comparison, Student's t-test for normal distribution with equal variance, Welch's t-test for normal distribution with unequal variance, or Wilcoxon rank-sum test for non-normal distribution were employed. Three-group and multi-group comparisons utilized one-way ANOVA for normal distribution with equal variance, Welch's ANOVA for normal distribution with unequal variance, or Kruskal-Wallis test for non-normal distribution, followed by post-hoc analyses of Tukey HSD for ANOVA, Dunn-Bonferroni test for Kruskal-Wallis when significant differences emerged as *P* less than 0.05. Categorical variables were analyzed using Pearson χ^2 (expected frequencies > 5), Yates'

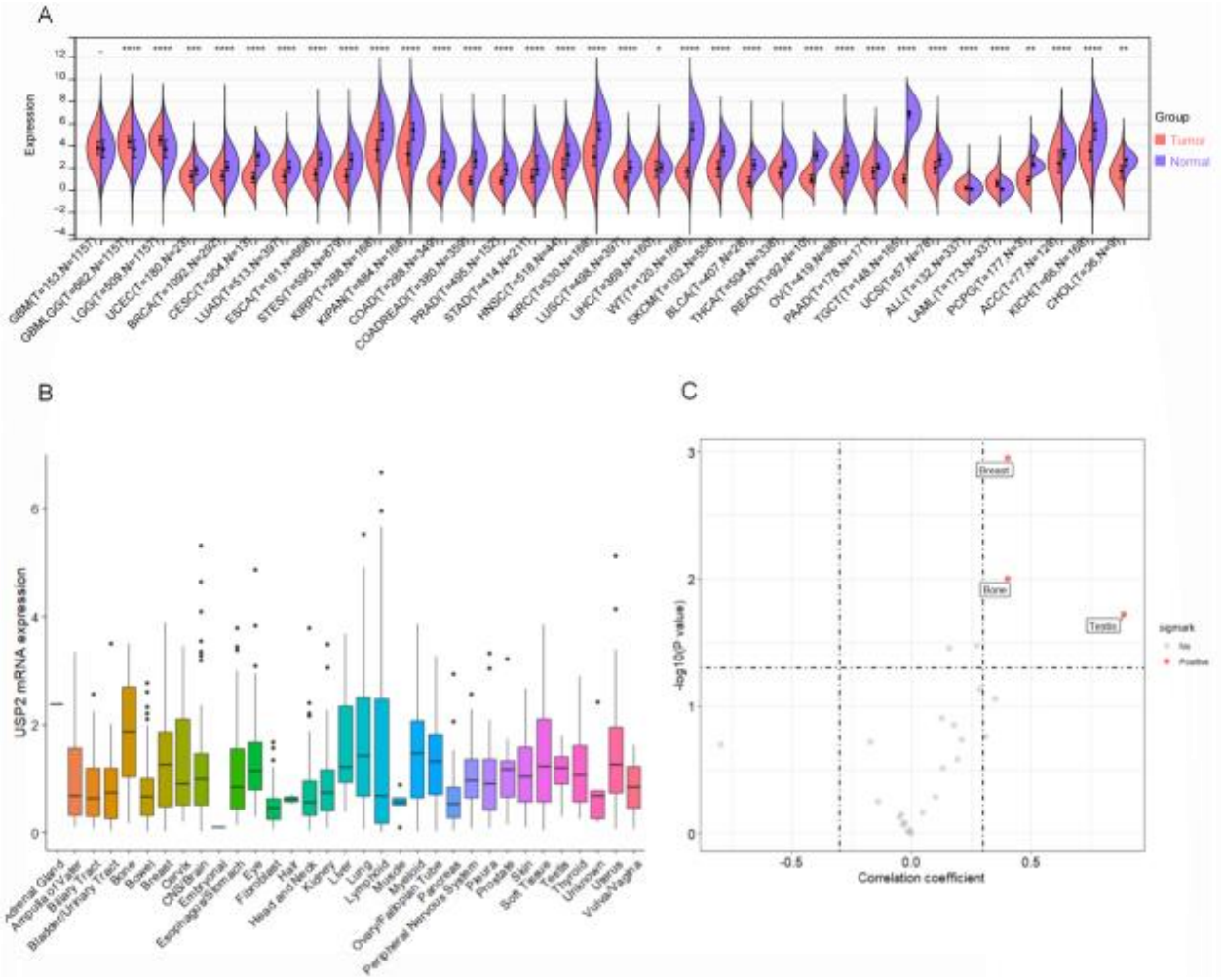

Figure 1. Specific expression map of USP2 in pan-cancer tissues. **(A)** The differential expression of usp2 in cancer tissues and normal tissues in TCGA and GTEx databases (***$P < 0.001$, **$P < 0.01$, *$P < 0.05$). **(B)** The expression of USP2 in 33 tissues in the CCLE database. **(C)** Correlation between expression of USP2 and copy number variation in the CCLE database.

corrected χ^2 (expected frequencies 1 - 5), or Fisher's exact test (expected frequencies < 1 or sample size < 40). *P* values less than 0.05, 0.01, and 0.001 were defined as statistically significant, very significant, and extremely significant differences.

Results and discussion

Tissue-specific expression of USP2 in a pan-cancer dataset

The expression levels of USP2 between tumor and normal tissues in 34 types of cancer in the TCGA and GTEx datasets were compared (Figure 1). The results showed that USP2 was expressed in all cancers, which suggested that USP2 could potentially be a tumor suppressor gene. The expression level of USP2 was the highest in normal tissues of kidney chromophobe (KICH), kidney renal papillary cell carcinoma (KIRP), and kidney renal clear cell carcinoma (KIRC) with the expression levels in normal tissues significantly higher than that in tumor tissues ($P < 0.001$). The expression of USP2 was also at a relatively high level in glioblastoma multiforme (GBM) and mesothelioma (MESO), while the lowest trend of which was in bladder urothelial carcinoma (BLCA) and acute myeloid leukemia (LAML). Except for adrenocortical carcinoma (ACC), lymphoid

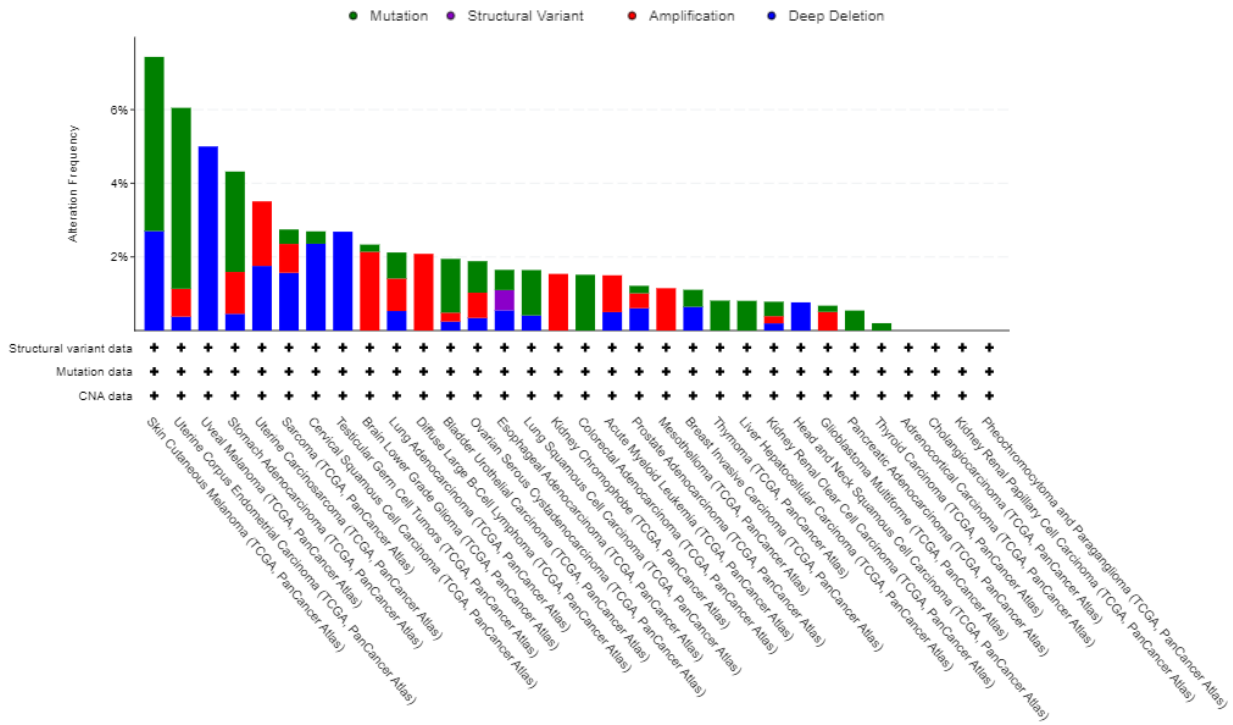

Figure 2. Genetic variations of USP2 based on the cBioPortalWeb database.

neoplasm diffuse large B-cell lymphoma (DLBC), LAML, brain lower grade glioma (LGG), mesothelioma (MESO), ovarian serous cystadenocarcinoma (OV), skin cutaneous melanoma (SKCM), testicular germ cell tumors (TGCT), uterine carcinosarcoma (UCS), and uveal melanoma (UVM), whose data were unavailable or too limited, there were significant differences in the expression of USP2 between tumor tissues and normal tissues in the remaining 18 cancers, and the expression of USP2 in tumor tissues was lower than that in normal tissues. USP2 was found in BLCA, KICH, KIRC, KIRP, breast invasive carcinoma (BRCA), colon adenocarcinoma (COAD), head and neck squamous cell carcinoma (HNSC), lung adenocarcinoma (LUAD), lung squamous cell carcinoma (LUSC), prostate adenocarcinoma (PRAD), rectum adenocarcinoma (READ), stomach adenocarcinoma (STAD), thyroid carcinoma (THCA), uterine corpus endometrial carcinoma (UCEC) with extremely significantly lower expression in tumor tissues than that in normal tissues ($P < 0.001$). The expression of USP2 in tumor tissues in GBM, pheochromocytoma, and paraganglioma (PCPG) was significantly lower than that in normal tissues ($P < 0.01$). The expression trend in cervical endocervical adenocarcinoma and squamous cell carcinoma (CESC), and cholangiocarcinoma (CHOL) also showed the same difference ($P < 0.05$). Besides, USP2 mRNA expression levels were not significantly different between tumor tissues and corresponding normal tissues in liver hepatocellular carcinoma (LIHC), pancreatic adenocarcinoma (PAAD), sarcoma (SARC), esophageal carcinoma (ESCA), thymoma (THYM) (Figure 1A).

Epigenetic alterations of USP2 in pan-cancer

The genetic alterations in the USP2 gene in different types of tumors in the TCGA dataset were studied on cBioPortalWeb. The results showed that USP2 gene mutation frequency was the highest (7.43%) in SKCM. Among all kidney cancers, “amplification” of the USP2 was the major alteration in KICH. In KIRC, “deep deletions”, “amplifications”, and “mutations” of the USP2 gene had been found, but mutations were the predominant type (Figure 2). USP2

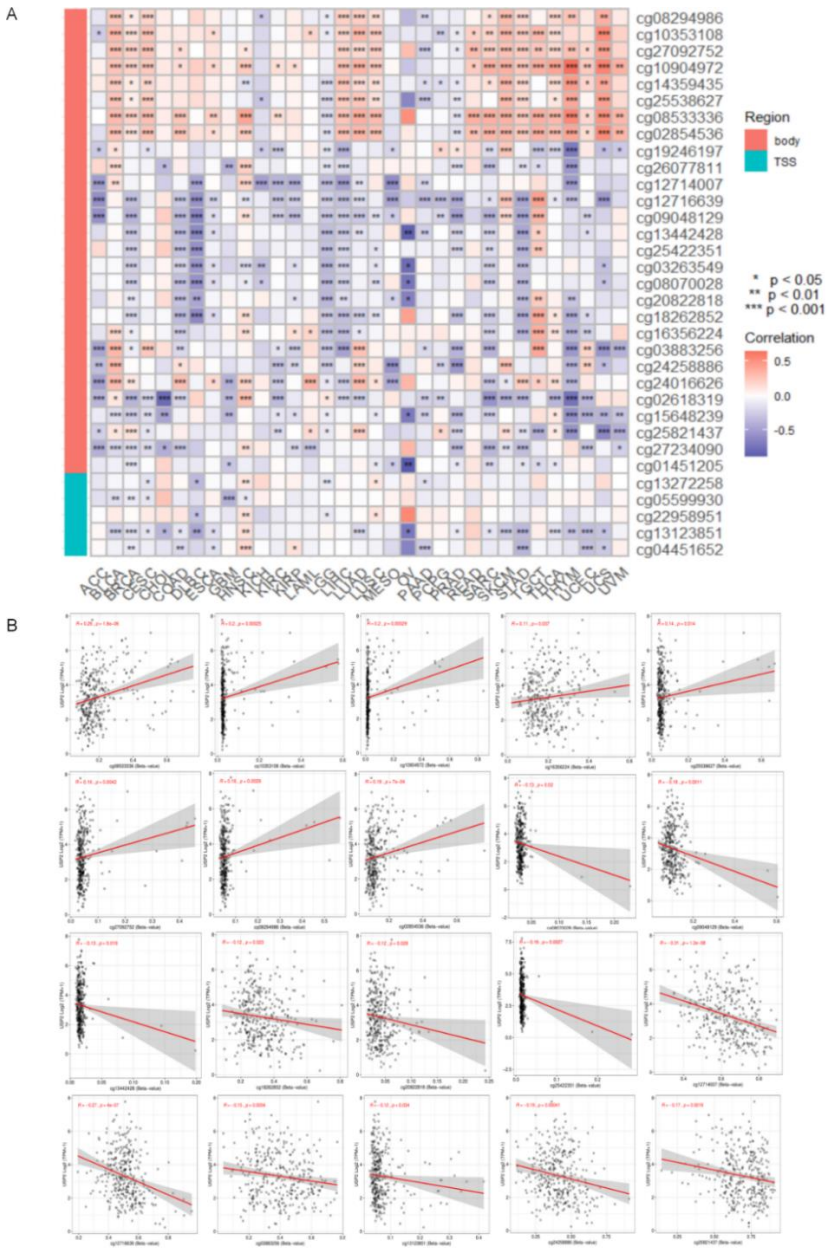

Figure 3. USP2 methylation levels based on TCGA data samples. **(A)** Heatmap of USP2 methylation site expression in the TCGA pan-cancer dataset. **(B)** The USP2 DNA methylation status of KIRC patients in the SMART App and MethSurv database.

methylation expression data obtained from the TCGA pan-cancer dataset were compared for differential analysis of methylation sites, and methylation probe sites were annotated and visualized (Figure 3). For probes in the USP2 gene promoter region (cg08070028, cg09048129, cg13442428, cg18262852, cg20822818, cg25422351, cg03883256, cg13123851, cg25821437), DNA methylation level (β value) was negatively correlated with USP2 expression level, while cg16356224 had the opposite trend. The probes for non-coding region of USP2 gene (cg10353108, cg10904972, cg27092752, cg08294986) demonstrated positively correlated with the expression level of USP2. The methylation of the probe (cg08533336, cg25538627, cg02854536) in the gene body region of USP2 showed a positive correlation

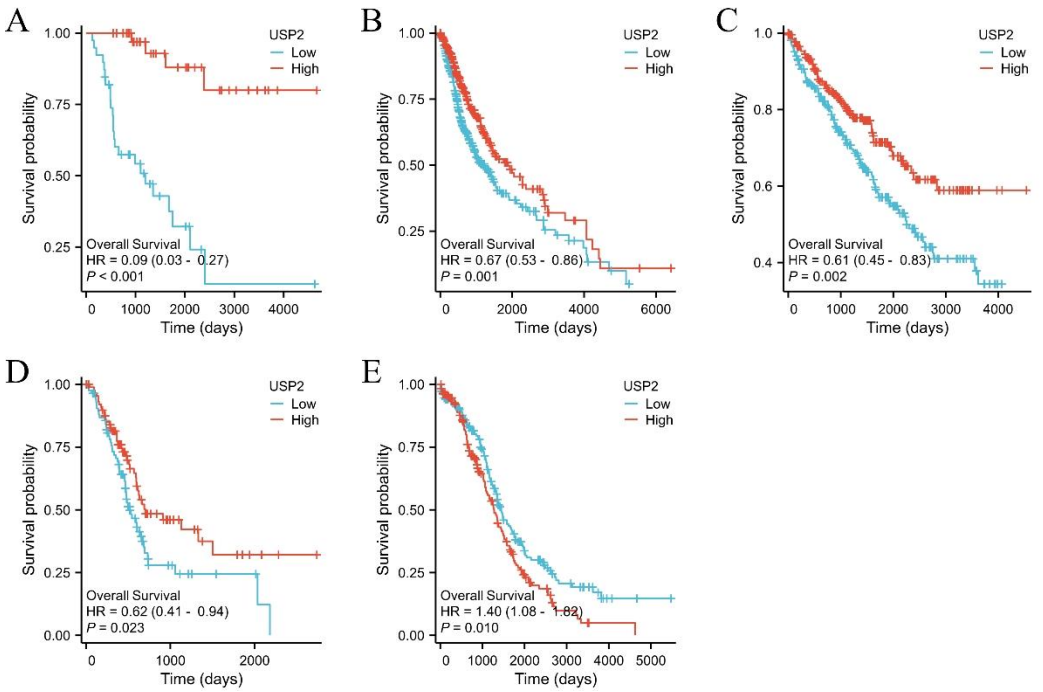

Figure 4. The prognostic value of USP2 expression for overall survival (OS) across different tumor types. **(A)** ACC. **(B)** GBMLGG. **(C)** KIRC. **(D)** PAAD. **(E)** OV.

with USP2 gene expression, while other probes (cg12714007, cg12716639, cg24258886) showed a negative correlation with USP2 gene expression (Figure 3B). The high methylation levels at the cg13442428, cg25422351, and cg03883256 sites in the promoter region of the USP2 gene were associated with a good prognosis ($P < 0.05$), while high methylation at the cg10353108, cg10904972, cg08533336, cg25538627, cg02854536, cg12714007, and cg12716639 sites in the non-coding region of the USP2 gene was associated with a poor prognosis ($P < 0.05$).

Prognostic value of USP2 expression in tumor tissues

The proportional hazards assumption test and fitted survival regression were performed using the "survival" package with results visualized using the "survminer" package and "ggplot2". The RNAseq data from the TCGA-KIRC project's STAR process were downloaded and organized from the TCGA database (https://portal.gdc.cancer.gov) in TPM format as well as the clinical data. Based on USP2 expression levels in different tumors, the relationship between USP2 expression and the prognosis of cancer patients was studied. The results showed that USP2 expression was significantly associated with overall survival (OS) in patients with five cancer types (Figure 4). High expression of USP2 was associated with good prognosis and OS in patients with ACC, GBMLGG, PAAD, and KIRC. Conversely, it was associated with poor prognosis and OS in patients with OV. The results suggested that the level of USP2 expression was highly correlated with disease prognosis in cancer research.

USP2 is an independent prognostic factor for patients with KIRC

The analysis found that KIRC patients with high USP2 expressions had significantly better OS than those with low expressions. Furthermore, the Cox model confirmed that USP2 had the potential to be a prognostic factor for patients with KIRC. The univariate Cox regression analysis showed that USP2 expression (low *vs*. high, HR = 0.611, 95% CI: 0.449 - 0.831, $P = 0.002$), T stage (T1 *vs*.

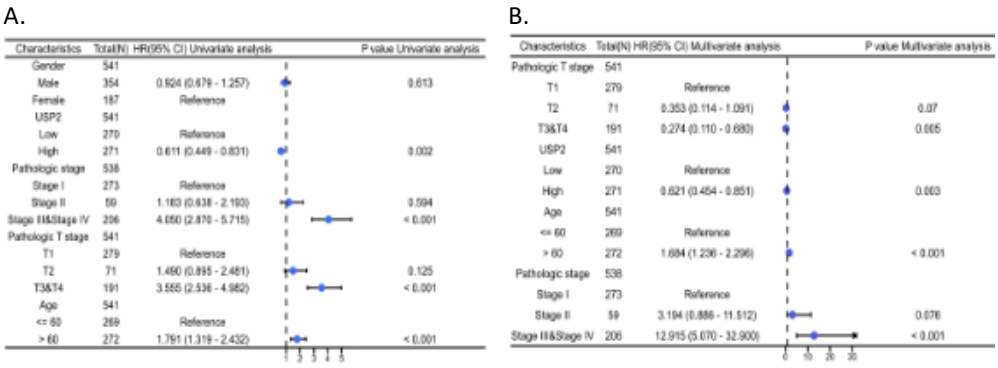

Figure 5. High expression of USP2 was an independent prognostic factor for patients with KIRC. **(A)** Forest plot of univariate Cox regression analysis of USP2 mRNA expression and OS in KIRC with different clinical pathological features. **(B)** Forest plot of multivariate Cox regression analysis of USP2 mRNA expression and OS in KIRC with different clinical pathological features.

Table 1. Clinical and genetic characteristics of KIRC patients in the TCGA cohort.

Characteristics		Low expression of USP2	High expression of USP2	*P* value
Number		270	271	
Age	≤ 60	140 (25.9%)	129 (23.8%)	0.322846301
	> 60	130 (24%)	142 (26.2%)	
Gender	Female	74 (13.7%)	113 (20.9%)	< 0.001
	Male	196 (36.29%)	158 (29.2%)	
Race	Asian	3 (0.6%)	5 (0.9%)	0.022419234
	African American	19 (3.6%)	38 (7.1%)	
	White	244 (45.7%)	225 (42.1%)	
Pathologic T stage	T1	121 (22.4%)	158 (29.2%)	0.005563901
	T2	43 (7.9%)	28 (5.2%)	
	T3 and T4	106 (19.6%)	85 (15.7%)	
Pathological stage	Stage I	118 (21.9%)	155 (28.8%)	0.005664558
	Stage II	35 (6.5%)	24 (4.5%)	
	Stage III and Stage IV	116 (21.6%)	90 (16.7%)	
Histological grade	G1	3 (0.6%)	11 (2.1%)	0.007289236
	G2	110 (20.6%)	126 (23.6%)	
	G3	104 (19.5%)	103 (19.3%)	
	G4	49 (9.2%)	27 (5.1%)	

T3 & T4, HR = 3.555, 95% CI: 2.536 - 4.982, $P \leq 0.001$), pathological stage (stage I *vs*. stage III & stage IV, HR = 4.050, 95% CI: 2.870 - 5.715, P ≤ 0.001), and Age (≤ 60 *vs*. > 60, HR = 1.791, 95% CI: 1.319 - 2.432, $P \leq 0.001$) were related to OS (Figure 5A). The multivariate Cox regression analysis showed that USP2 expression (HR = 0.621, 95% CI: 0.454 – 0.851, $P = 0.003$) was an independent prognostic factor for OS in KIRC (Figure 5B).

Expression of USP2 mRNA and clinical features in KIRC

The clinical and genetic features of KIRC patients in the TCGA cohort were summarized in Table 1. The patients were grouped by the high or low expression of USP2 and then divided into USP2 high expression group and USP2 low expression group. There were differences between these two groups in terms of T stage, pathological stage, gender, race, and prognosis survival. High expression of USP2 was associated with T1 stage

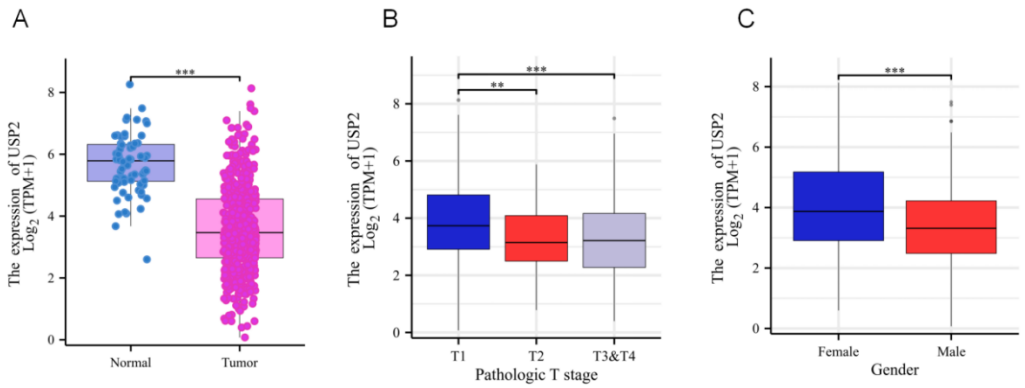

Figure 6. Expression of USP2 and clinical characteristics of KIRC patients. **(A)** Expression levels of USP2 between normal subjects and KIRC patients. **(B)** Effect of T stage on USP2 expression levels in KIRC patients. **(C)** Effect of gender on USP2 expression levels in KIRC patients.

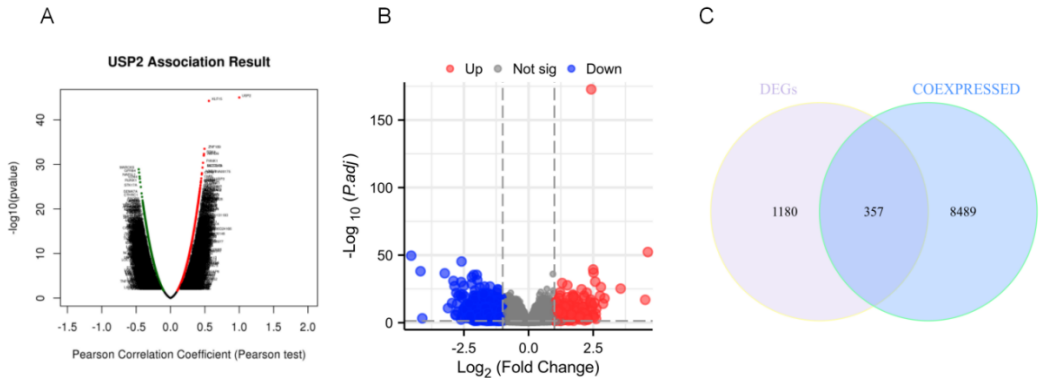

Figure 7. Co-expressed genes related to USP2 in KIRC. **(A)** Using LinkedOmics to analyze co-expressed genes associated with USP2 expression and volcano plots result. **(B)** Volcano plot of differentially expressed genes (DEGs) between the USP2 High group and the USP2 low group. **(C)** Venn diagram of intersecting genes between significantly co-expressed genes of USP2 and significant DEGs.

(*P* = 0.006) and Stage I (*P* = 0.006), while low expression was associated with T2, T3, T4 stages (*P* = 0.006) and Stages II, III, IV (*P* = 0.006). Furthermore, high expression of USP2 was significantly correlated with good prognosis survival (*P* < 0.001). Based on the T stage, the differential expression of USP2 in KIRC patients was analyzed. USP2 was underexpressed in KIRC patients and overexpressed in healthy individuals (Figure 6A). According to the NCCN staging criteria for KIRC, the expression of USP2 in T1 stage KIRC patients was higher than that in T2 stage (*P* < 0.01) and T3, T4 stages (*P* < 0.001) (Figure 6B). Additionally, the expression level of USP2 was higher in female patients compared to males (*P* < 0.001) (Figure 6C).

Analysis of USP2 co-expression genes in KIRC patients

To further investigate the mechanism of USP2 in the development of KIRC, LinkedOmics was used to study the genes co-expressed with USP2 in KIRC patients (Figure 7A). The results showed that a total of 8,846 co-expressed genes in KIRC were significantly related to USP2 (FDR < 0.05, *P* < 0.05, |cor.| ≥ 0.3). Among these genes, 3,345 genes were positively correlated with USP2 expression while the others were negatively correlated (Figure 7B). Subsequently, DEGs were identified between the USP2 high group and USP2 low group in KIRC samples. A total of 1,541 DEGs were identified (*P* < 0.05, $|\log_2 Fc| \geq 1$). Comparing these 1,541 USP2-related DEGs with the above 8,846 significantly co-expressed genes,

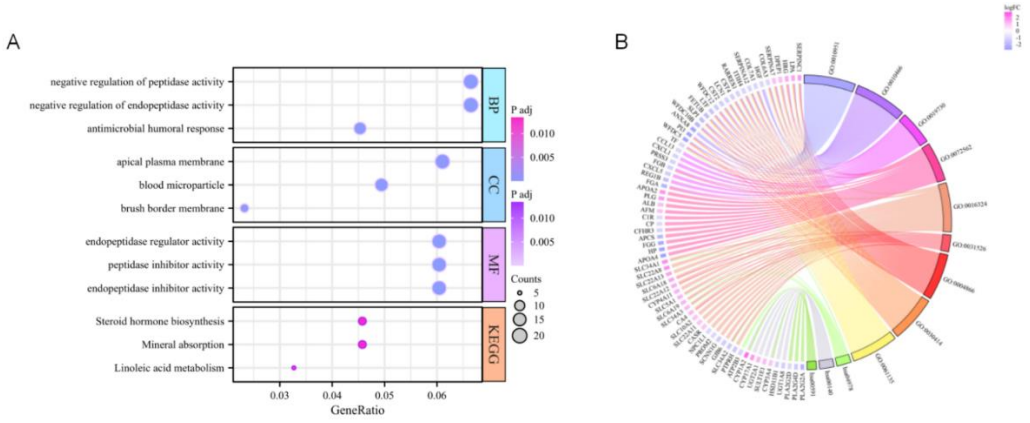

Figure 8. 357 KEGG/GO analysis of intersection genes.

357 intersection genes were obtained (Figure 7C) and further functional analysis were performed.

Functional enrichment analysis of USP2 in KIRC

To study the biological functions of the 357 overlapping genes, the differential gene sets and corresponding logFC values were first sorted out. After converting the inputmolecule list to IDs, the "clusterProfiler" package was used for enrichment analysis. The z-score value corresponding to each enrichment entry was calculated using the 'GOplot' package, and the visualization was performed using the 'GGplot' package. The top 12 pathways with the highest enrichment were shown in Figure 8. USP2 and its related genes mainly regulate the body's immune function by modulating the activity of peptidases and endopeptidases. These pathways include negative regulation of peptidase activity, negative regulation of endopeptidase activity, peptidase inhibitor activity, endopeptidase inhibitor activity. In addition, there are still pathways related to immune regulation such as antimicrobial humoral response. The differential genes between the high and low USP2 expression groups were converted into IDs, and GSEA analysis was performed using the "clusterProfiler" package. A total of 9 pathways were selected with FDR (Q value) < 0.25 and *P* adjust < 0.05. The 4 pathways with nes > 2 and the 5 pathways with nes < -2 were visualized. Through GO/KEGG and GSEA analysis study showed that USP2 primarily exerted its immune function in the progression of KIRC by regulating the activity of peptidases and endopeptidases [26, 27], while also playing a regulatory role in humoral immunity. By using GSEA analysis, the significantly altered molecular pathways between the USP2 high group and the USP2 low group in the KIRC dataset were explored (Figure 9). The results showed that USP2 could regulate immune-related processes or pathways such as folate metabolism [28-30], selenium micronutrient networks [31], innate immune system [32], signaling by interleukins [33], and metabolism of lipids [34, 35].

PPI interaction network of USP2 and intersection gene sets

The STRING database was used to analyze the PPI network of overlapping genes, and the PPI network diagram was generated in Figure 10A. When the 357 intersecting genes were added to the USP2 input ID list, a total of 269 nodes and 954 edges were obtained. The MCODE plugin in Cytoscape software was used to further analyze the PPI network to screen for hub genes. The MCODE analysis showed that the most important module (MCODE score = 10.727) was composed of 12 central genes (Figure 10B) with a total of 12 nodes and 59 edges. Among them, the expression of CP, ITIH4, and TF in KIRC tumor tissues was extremely significantly higher than that in normal tissues (*P* < 0.001). The expressions of TTR, PLG, LPA, HRG, SERPINC1, APOA2, ALB, and AFM in KIRC tumor tissues were

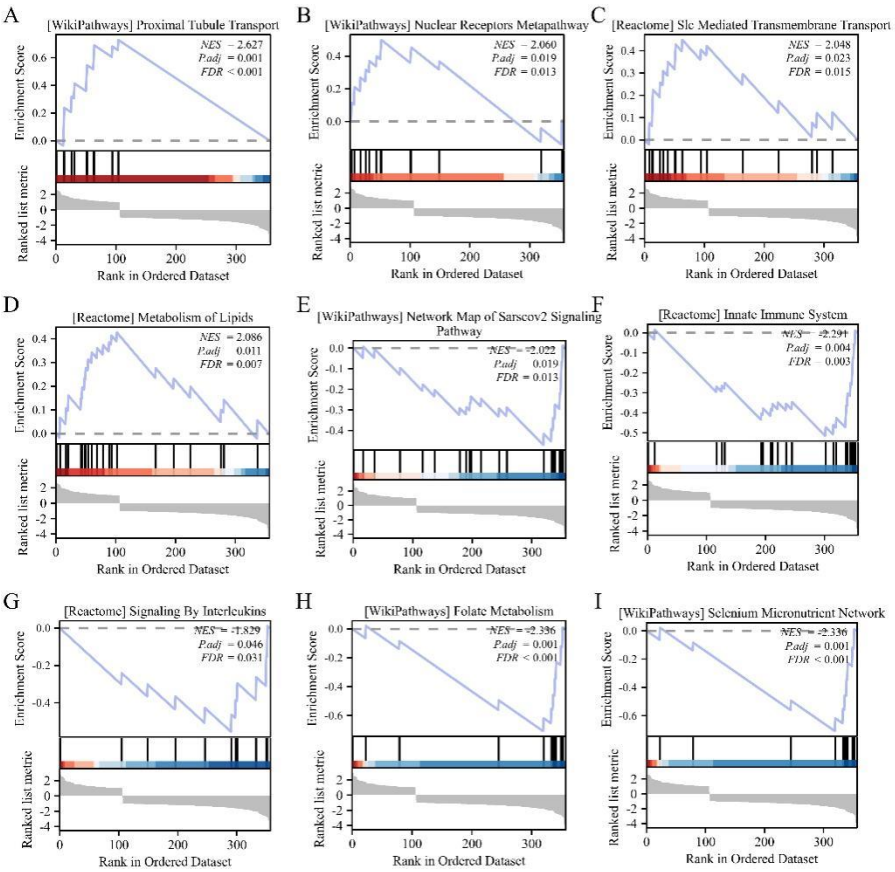

Figure 9. GSEA enrichment analysis results for differential genes between the expression of USP2 on high and low groups in KIRC. **(A)** Proximal tubule transport. **(B)** Folate metabolism. **(C)** Selenium micronutrient network. **(D)** Innate immune system. **(E)** Metabolism of lipids. **(F)** Nuclear receptors metapathway. **(G)** Network map of sarscov2 signaling pathway. **(H)** SLC mediated transmembrane transport. **(I)** Signaling by interleukins.

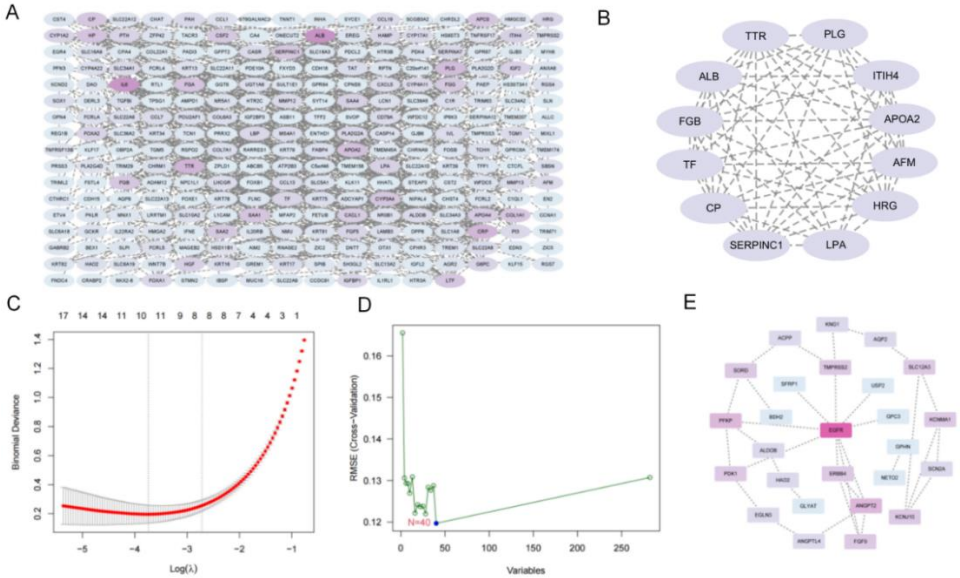

Figure 10. Study on PPI interaction network related to USP2. **(A)** PPI interaction network of USP2 with 357 intersecting genes. **(B)** Hub gene interaction network screened by MCODE. **(C)** Combined LASSO method for screening KIRC characteristic genes in GSE datasets. **(D)** Combined SVM method for screening KIRC characteristic genes in GSE datasets. **(E)** Interaction network of KIRC characteristic genes with USP2.

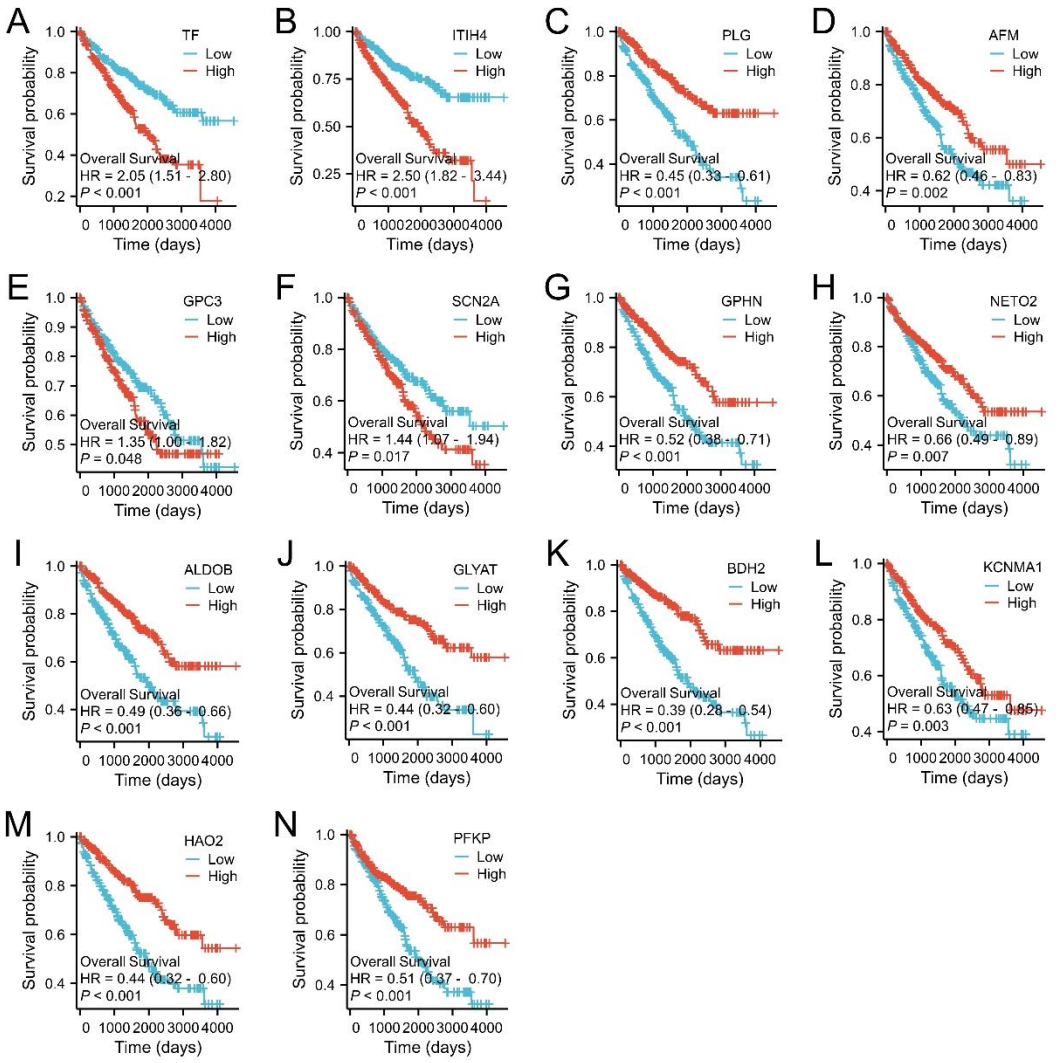

Figure 11. The OS situation of USP2-related genes in KIRC. **(A)** TF. **(B)** ITIH4. **(C)** PLG. **(D)** AFM. **(E)** GPC3. **(F)** SCN2A. **(G)** GPHN. **(H)** NETO2. **(I)** ALDOB. **(J)** GLYAT. **(K)** BDH2. **(L)** KCNMA1. **(M)** HAO2. **(N)** PFKP.

extremely significantly lower than that in normal tissues ($P < 0.001$). High expression of ITIH4 and TF genes was significantly associated with poor overall survival in KIRC patients, whereas elevated levels of PLG and AFM genes correlate with good overall survival. In addition, the "lasso" and "svm" packages in R were used to screen for disease characteristic genes in the transcriptome sequencing datasets GSE781 and GSE53000 (Figure 10C, 10D), which were contained KIRC tumor tissues and normal tissues sample in the GEO (https://www.ncbi.nlm.nih.gov/geo/). A total of 43 disease characteristic genes were obtained. And then, a PPI interaction network of USP2 and disease characteristic genes was constructed, and 26 nodes and 32 edges were obtained (Figure 10E). The high expression of GPC3 and SCN2A was associated with poor OS in patients ($P < 0.01$), while GPNH, ALDOB, GLYAT, BDH2, HAO2, PFKP ($P < 0.001$), NETO2 and KCNMA1 ($P < 0.01$) were associated with good OS in patients (Figure 11).

Immune-related analysis

The standardized pan-cancer dataset, TCGA TARGET GTEx (PANCAN, N = 19,131, G = 60,499), was downloaded, and the expression data of the USP2 gene were extracted. 150 marker genes

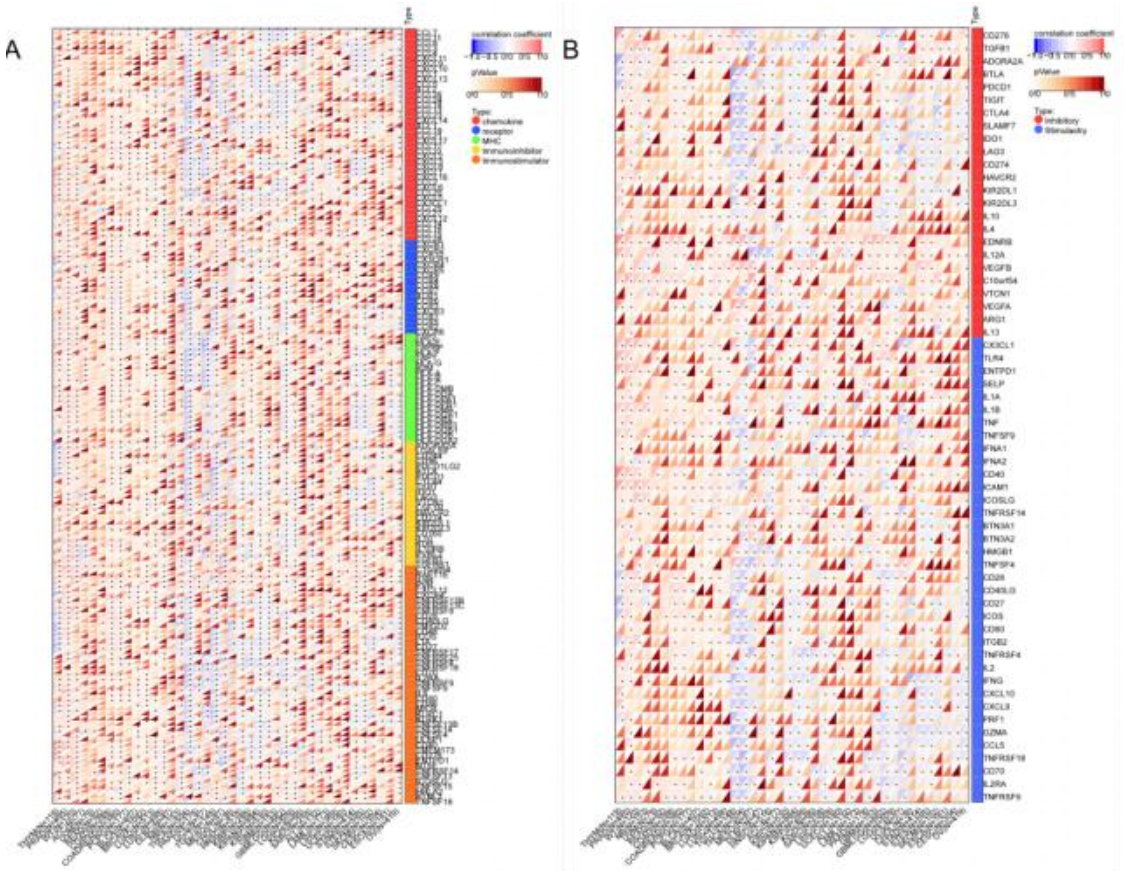

Figure 12. Analysis of USP2 and immune-related genes in KIRC. **(A)** Analysis of USP2 and immune regulation-related genes. **(B)** Analysis of USP2 and immune checkpoint genes.

from five types of immune pathways including chemokine (41), receptor (18), MHC (21), immunoinhibitor (24), immunostimulator (46) from each sample were selected from primary solid tumor, primary tumor, primary blood derived cancer - bone marrow, primary blood derived cancer - peripheral blood. All normal samples were filtered, and a $\log_2(x+1)$ transformation for each expression value was performed. The Pearson correlation between USP2 (ENSG00000036672) and the marker genes of the five immune pathways were calculated. The results showed that USP2 was negatively correlated with most immune genes in the sample information of 530 KIRC patients. The expression of USP2 was related to the expression of most immune-related genes. In KIRC, the expression of USP2 was related to immune regulatory genes of ICOSLG, HHLA2, CD274, CD96, HLA-DOB, CCL7, CXCR1 (Figure 12A). Using the same data processing method, the correlation between USP and six types of immune checkpoint pathway genes was checked including inhibitory (24) and stimulatory (36) [36]. The results found that USP2 showed a negative correlation trend with most immune checkpoint pathway genes (Figure 12B). Immune checkpoint genes included TGFB1, BTLA, IL10, CX3CL1, CD27. Overall, USP2 was involved in the relevant immunological processes of KIRC.

Immune infiltration analysis

In recent years, scientific research has discovered that immune infiltration is associated with the occurrence, development, and metastasis of human cancers [37]. This study extracted the gene expression profiles of each tumor, mapped the gene profiles, and calculated the

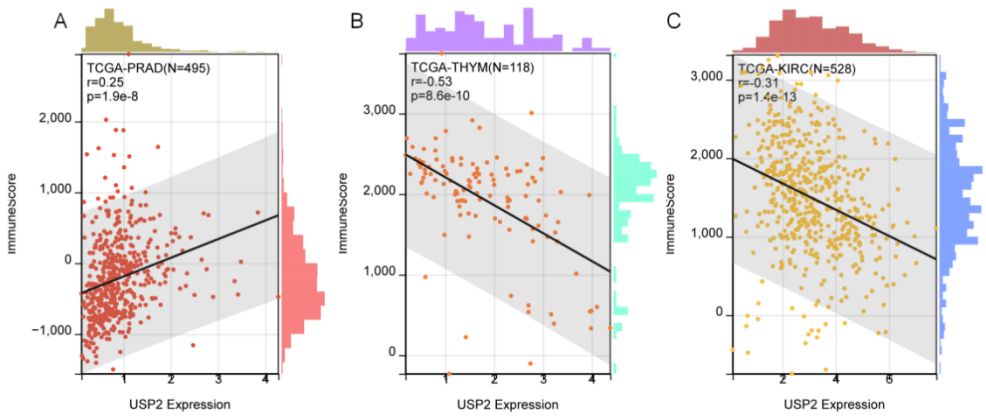

Figure 13. Analysis of USP2 in regulating immune cell infiltration. **(A)** The correlation between USP2 expression and immune infiltration in PRAD. **(B)** The correlation between USP2 expression and immune infiltration in THYM. **(C)** The correlation between USP2 expression and immune infiltration in KIRC.

immunescore for each patient in all tumors. The Pearson's correlation coefficient between gene expression and immune infiltration scores in each tumor was calculated to identify significantly correlated immune infiltration scores. The results demonstrated that the expression of USP2 was significantly correlated with immune infiltration in 21 cancer types, 4 of which were positively correlated and 17 were negatively correlated with significant differences (Figure 13A, 13B). The cancer with the most positive correlation with USP2 expression was PRAD (r = 0.25), and the most negative correlation cancer was THYM (r = -0.53), among which KIRC and the expression of USP also had a negative correlation (r = -0.31) (Figure 13C). In the analysis of immune cells, the correlation between USP2 expression and different immune cell invasions in various cancer tissues was explored. In KIRC, KIRP, and LGG, the infiltration of Tregs cells was negatively correlated with USP2 expression. In addition, the infiltration of cancer-associated fibroblasts was negatively correlated with the expression of USP2 in KIRC and KIRP, while it was positively correlated in THYM and PRAD. The expression of USP2 was positively correlated with the infiltration of CD8+ T cells in PAAD and negatively correlated with TGCT (Figure 14). These findings suggested that USP2 might be a new immune-related tumor suppressor gene in KIRC. Additionally, there was no significant correlation between USP2 expression and the infiltration levels of neutrophils, eosinophils, mast cells, monocytes, or dendritic cells.

Expression of USP2 at the single-cell level

Single-cell transcriptome sequencing provides enormous potential for analyzing the potential functions of candidate molecules. In acute myeloid leukemia (AML), the expression of USP2 was positively correlated with DNA repair, and negatively correlated with differentiation, DNA damage, hypoxia, and quiescence. In the realm of BRCA, USP2 exhibited a positive correlation with all tumors' biological behaviors, encompassing angiogenesis, apoptosis, cell cycle, differentiation, DNA damage, DNA repair, EMT, hypoxia, inflammation, invasion, metastasis, proliferation, quiescence, and stemness. However, it manifested a negative correlation trend with all tumors' biological behaviors in LUAD. In particular, USP2 demonstrated a potent negative correlation with the oncological biological behavior of DNA damage within AML, retinoblastoma (RB), and uveal melanoma (UM). USP2 exhibited a positive association with the oncological DNA repair behavior in AML, whilst presenting a negative correlation in RB and UM (Figure 15A). Additionally, a high correlation between USP2 expression and the risk of affliction in BRCA, BLCA, LUSC, and HNSC were

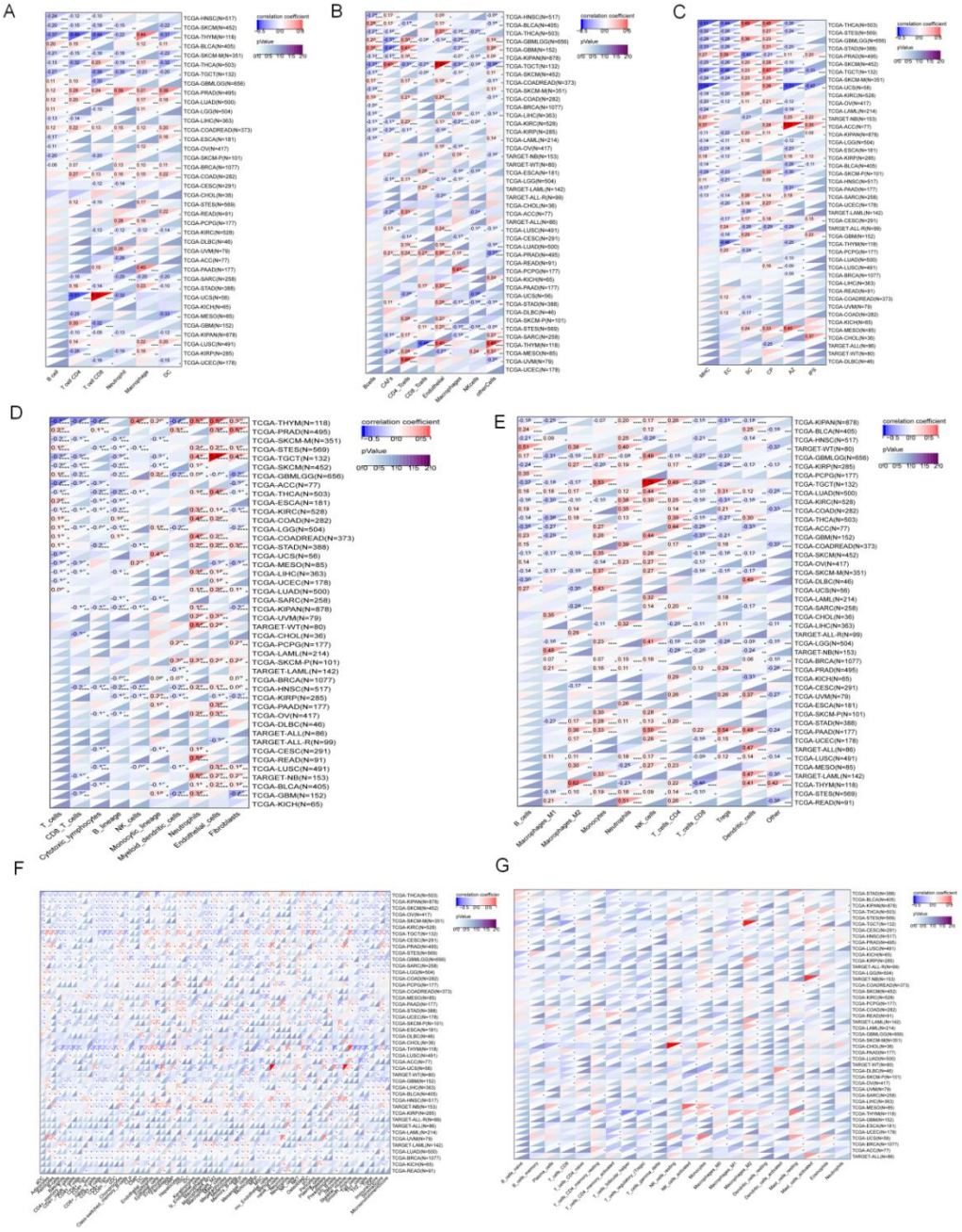

Figure 14. Expression of USP2 in different immune cells analyzed using various algorithms. **(A)** Timer algorithm. **(B)** EPIC algorithm. **(C)** IPS algorithm. **(D)** MCPcounter algorithm. **(E)** QUANTISEQ algorithm. **(F)** xCELL algorithm. **(G)** CIBERSORT algorithm.

found ($P < 0.05$) (Figure 15B). Contrastingly, a negative correlation was observed with the risk of affliction in ACC, KIRP, KIRC, PAAD, and MESO ($P < 0.05$). TISCH2 database (https://tisch.comp-genomics.org) was employed to analyze the expression of USP2 within diverse cellular types in the KIRC dataset. The results showed that, in KIRC data sets, the expression of USP2 was higher in regulating endothelial, fibroblasts, and malignant (Figure 15C). The KIRC_GSE171306 dataset was selected to further analyze the expression of USP2 in different cell populations. USP2 was primarily expressed within malignant, CD8T, Endothelial, Mono/Macro, and NK cells

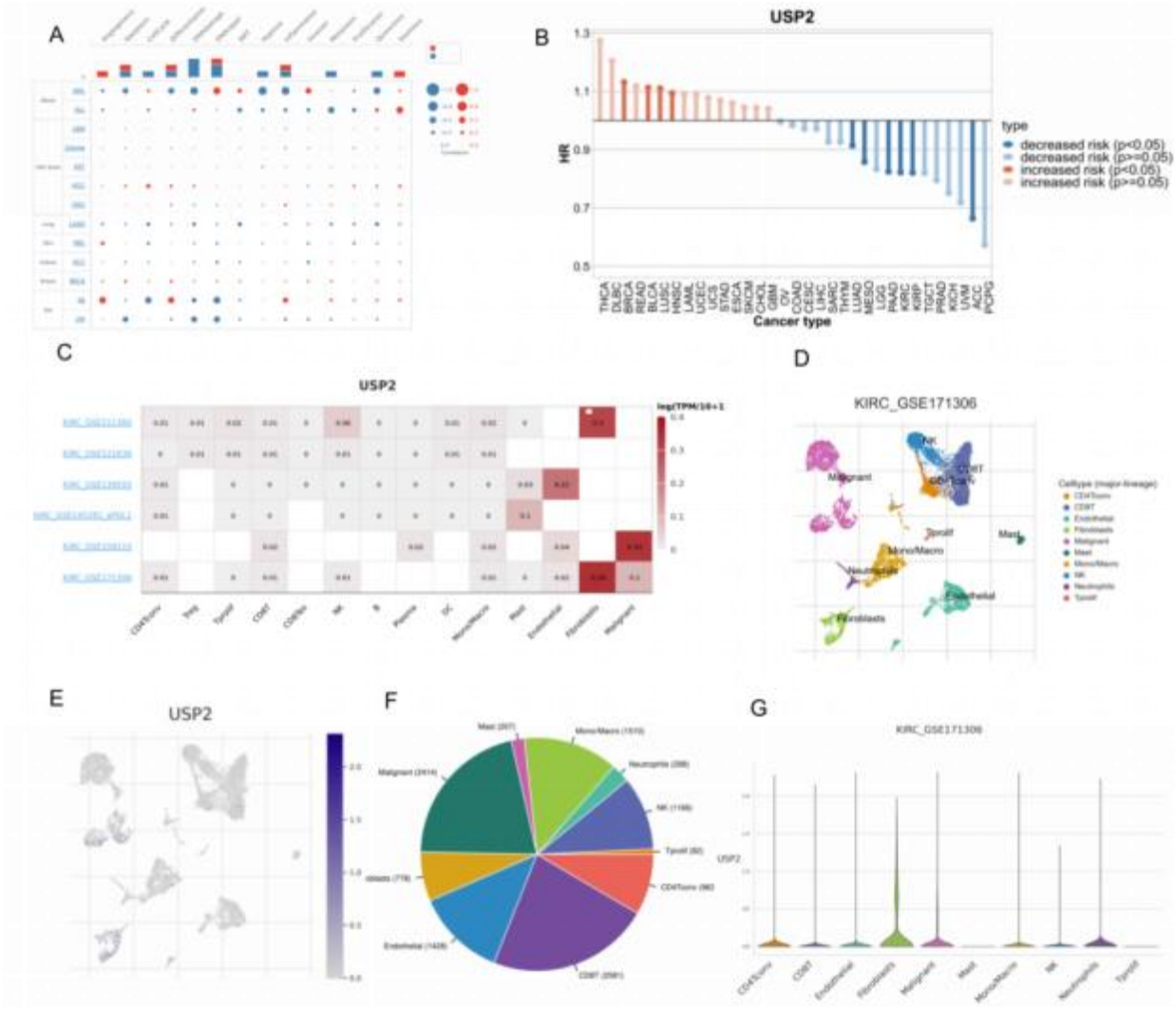

Figure 15. Expression of USP2 at the single-cell level. **(A)** Using the CancerSEA database to explore the correlation between USP2 and the biological behavior of cells in different tumor tissues. **(B)** Analysis of the risk relationship between different cancers and USP2 expressions based on the CancerSEA database. **(C)** Cellular USP2 expression in 6 KIRC single cell data sets in the TISCH2 database. **(D) to (G)** Single-cell sequencing analysis of the USP2 gene in GSE171306.

(Figure 15D to 15G). At present, the clinical diagnosis and treatment of renal carcinoma are well-established. KIRC represents the principal type of renal cancer, and the recurrence rate of radical nephrectomy for advanced renal clear cell carcinoma is 20 - 40%. A plenty of studies suggest that USP2 plays a pivotal regulatory role in processes such as tumor migration, apoptosis, and diffusion [38, 39]. The statistical results confirmed that the expression of USP2 in all cancers was significantly higher in normal tissues than in tumor tissues, which suggested that USP2 could potentially be a tumor suppressor gene. The CCLE database showed that USP2 had higher expression levels in bone and testes. Among KIRC cell lines, the NCIH2004RT cell line had the highest expression, while the KMRC1 cell line had the lowest expression (Figure 16). This study investigated the clinical significance and the role of USP2 in KIRC through bioinformatics analysis and predicted the role and mechanism of USP2 in the occurrence of KIRC through enrichment analysis. However, the specific mechanism of action and clinical application still need further verification.

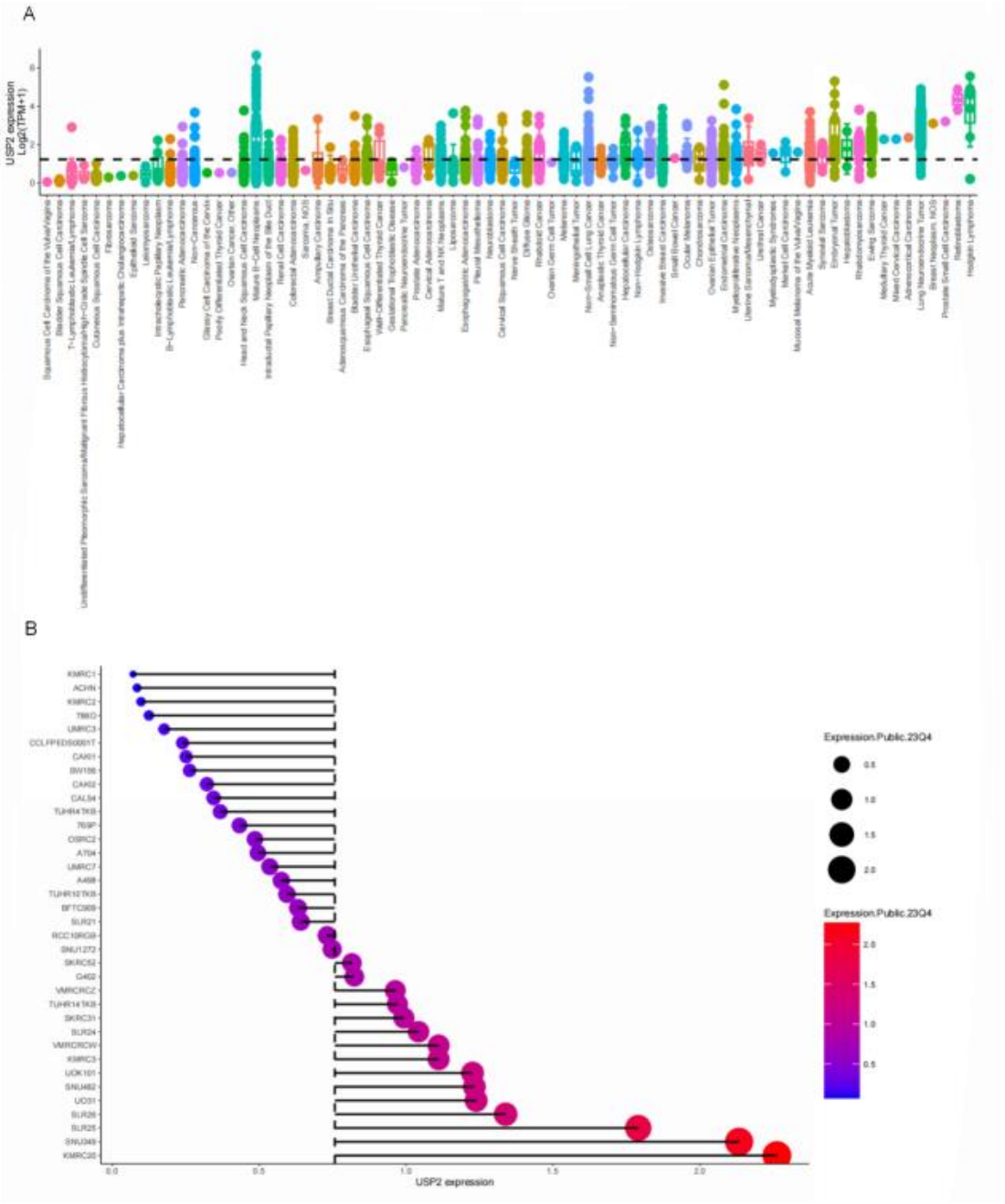

Figure 16. The expression of USP2 in tissues and cells in the CCLE database. **(A)** The expression of USP2 in 76 types of tumors in the CCLE database. **(B)** The expression of USP2 in renal cell carcinoma cell lines.

Acknowledgements

This work was partially supported by the "Open Competition Mechanism to Select the Best Candidates" project of the Key Science and Technology Program, Heilongjiang Province, China (Grant No. 2022ZXJ02C01).

References

1. Tian J, Xu T, Fan L, Sun H. 2025. Value of contrast-enhanced ultrasound in the diagnosis of clear cell renal cell carcinoma: A meta-analysis. J Clin Ultrasound. 53(2):343-352.
2. Wang G, Lv Q, Ma C, Zhang Y, Li H, Ding Q. 2021. SMARCC1 expression is positively correlated with pathological grade and

good prognosis in renal cell carcinoma. Transl Androl Urol. 10(1):236-242.
3. Dong K, Gu D, Shi J, Bao Y, Fu Z, Fang Y, et al. 2022. Identification and verification of m7G modification patterns and characterization of tumor microenvironment infiltration *via* multi-omics analysis in clear cell renal cell carcinoma. Front Immunol. 13:874792.
4. Wang W, Zhang F, Hu Y, Liu G. 2024. STING agonist, SMA-2, inhibits clear cell renal cell carcinoma through improving tumor microenvironment. Mol Cell Biochem. 479(7):1697-1705.
5. Cheng Y, Guo L. 2025. Lactate metabolism and lactylation in kidney diseases: Insights into mechanisms and therapeutic opportunities. Ren Fail. 47(1):2469746.
6. Harrigan JA, Jacq X, Martin NM, Jackson SP. 2018. Deubiquitylating enzymes and drug discovery: Emerging opportunities. Nat Rev Drug Discov. 17(1):57-78.
7. Park J, Cho J, Song EJ. 2020. Ubiquitin-proteasome system (UPS) as a target for anticancer treatment. Arch Pharm Res. 43(11):1144-1161.
8. Yang H, Ai H, Zhang J, Ma J, Liu K, Li Z. 2023. UPS: Opportunities and challenges for gastric cancer treatment. Front Oncol. 13:1140452.
9. Hoeller D, Hecker CM, Dikic I. 2006. Ubiquitin and ubiquitin-like proteins in cancer pathogenesis. Nat Rev Cancer. 6(10):776-788.
10. Mevissen TE, Hospenthal MK, Geurink PP, Elliott PR, Akutsu M, Arnaudo N, *et al*. 2013. OTU deubiquitinases reveal mechanisms of linkage specificity and enable ubiquitin chain restriction analysis. Cell. 154(1):169-184.
11. Yi J, Tavana O, Li H, Wang D, Baer RJ, Gu W. 2023. Targeting USP2 regulation of VPRBP-mediated degradation of p53 and PD-L1 for cancer therapy. Nat Commun. 14(1):1941.
12. Xiao W, Wang J, Wang X, Cai S, Guo Y, Ye L, *et al*. 2022. Therapeutic targeting of the USP2-E2F4 axis inhibits autophagic machinery essential for zinc homeostasis in cancer progression. Autophagy. 18(11):2615-2635.
13. Liu X, Zhang G, Liu L, Xiong G, Liu J, Wei W. 2025. USP2 promotes the proliferation and inflammation of fibroblast-like synovial cells in rheumatoid arthritis through deubiquitination of TRAF2. Biochem Genet. 63(1):592-605.
14. Kuang Z, Liu X, Zhang N, Dong J, Sun C, Yin M, *et al*. 2023. USP2 promotes tumor immune evasion *via* deubiquitination and stabilization of PD-L1. Cell Death Differ. 30(10):2249-2264.
15. Sacco JJ, Coulson JM, Clague MJ, Urbé S. 2010. Emerging roles of deubiquitinases in cancer-associated pathways. IUBMB Life. 62(2):140-157.
16. Gong Y, Li R, Zhang R, Jia L. 2025. USP2 reversed cisplatin resistance through p53-mediated ferroptosis in NSCLC. BMC Med Genomics. 18(1):39.
17. Zhang S, Guo Y, Zhang S, Wang Z, Zhang Y, Zuo S. 2023. Targeting the deubiquitinase USP2 for malignant tumor therapy (Review). Oncol Rep. 50(4):176.
18. Shu XF, Zhou Y. 2023. Pan-cancer analysis of CEMIP gene expression in human malignant tumors. Chin J Surg Oncol. 15(01):47-54.
19. Hu J, Yu A, Othmane B, Qiu D, Li H, Li C, *et al*. 2021. Siglec15 shapes a non-inflamed tumor microenvironment and predicts the molecular subtype in bladder cancer. Theranostics. 11(7):3089-3108.
20. Alfar R, Napoleon JV, Shahriar I, Finnell R, Walchle C, Johnson A, *et al*. 2023. Selective reprogramming of regulatory T cells in solid tumors can strongly enhance or inhibit tumor growth. Front Immunol. 14:1274199.
21. Hamed A, Ghareeb D, Mohamed TM, Hamed M, Nofal MS, Gaber M. 2023. Caffeine-folic acid-loaded-chitosan nanoparticles combined with methotrexate as a novel HepG2 immunotherapy targeting adenosine A2A receptor downstream cascade. BMC Complement Med Ther. 23(1):384.
22. Liu X, Chen C, Xu P, Chen B, Xu A, Liu C. 2023. Development and experimental validation of a folate metabolism-related gene signature to predict the prognosis and immunotherapeutic sensitivity in bladder cancer. Funct Integr Genomics. 23(4):291.
23. Diwakar BT, Korwar AM, Paulson RF, Prabhu KS. 2017. The regulation of pathways of inflammation and resolution in immune cells and cancer stem cells by selenium. Adv Cancer Res. 136:153-172.
24. Lyu DW. 2024. Immunomodulatory effects of exercise in cancer prevention and adjuvant therapy: A narrative review. Front Physiol. 14:1292580.
25. Jacobse J, Pilat JM, Li J, Brown RE, Kwag A, Buendia MA, *et al*. 2024. Distinct roles for interleukin-23 receptor signaling in regulatory T cells in sporadic and inflammation-associated carcinogenesis. Front Oncol. 13:1276743.
26. Long Y, Shi H, He Y, Qi X. 2024. Analyzing the impact of metabolism on immune cells in tumor microenvironment to promote the development of immunotherapy. Front Immunol. 14:1307228.
27. Li CF, Lian LL, Li QR, Jiao Y. 2024. Immunotherapy for metastatic gastric cancer. World J Gastrointest Surg. 16(11):3408-3412.
28. Kitamura H, Hashimoto M. 2021. USP2-related cellular signaling and consequent pathophysiological outcomes. Int J Mol Sci. 22(3):1209.
29. Lee TG, Woo SM, Seo SU, Kim S, Park JW, Chang YC, *et al*. 2023. Inhibition of USP2 enhances TRAIL-mediated cancer cell death through downregulation of survivin. Int J Mol Sci. 24(16):12816.
30. Tu R, Ma J, Zhang P, Kang Y, Xiong X, Zhu J, *et al*. 2022. The emerging role of deubiquitylating enzymes as therapeutic targets in cancer metabolism. Cancer Cell Int. 22(1):130.
31. Wei C, Zhao X, Zhang H, Wang L. 2023. USP2 promotes cell proliferation and metastasis in choroidal melanoma *via* stabilizing Snail. J Cancer Res Clin Oncol. 149(11):9263-9276.
32. Agrawal P, Olgun G, Singh A, Gopalan V, Hannenhalli S. 2024. Characterizing the pan-cancer role of exosomal miRNAs in metastasis across cancers. Comput Struct Biotechnol J. 27:252-264.
33. Chen W, Ji Y, Wang R, Ji R, Lin Y, Wu Y, *et al*. 2024. Investigating POU3F4 in cancer: expression patterns, prognostic implications, and functional roles in tumor immunity. Heliyon. 11(1):e41587.
34. Alekseeva AO, Zolotovskaia MA, Sorokin MI, Suntsova MV, Zakharova GS, Pugacheva PA, *et al*. 2024. The first multiomics association study of trace element and mineral concentration and RNA sequencing profiles in human cancers. Biochemistry (Mosc). 89(12):2274-2286.

35. Hu Y, Qin S, Deng R. 2025. Impact of glioma metabolism-related gene ALPK1 on tumor immune heterogeneity and the regulation of the TGF-β pathway. Front Immunol. 15:1512491.
36. Liu Q, Sun S, Zhou C, Xu H. 2025. Comprehensive analysis of the prognostic, immunological, and diagnostic roles of SIRT1 in pan-cancer and its validation in KIRC. Front Immunol. 15:1501867.
37. Shen N, Fan C, Ying H, Li X, Zhang W, Yu J, *et al*. 2025. Exploration of ANKRD27 as an immune-related prognostic factor in pan-cancer and hepatocellular carcinoma. Front Oncol. 14:1511240.
38. Xiao K, Li X, Ullah I, Hu W, Wang K, Yang F, *et al*. 2025. Unveiling the role of ASPP1 in cancer progression: Pan-cancer bioinformatics and experimental validation in colorectal cancer. Front Oncol. 14:1529809.
39. Zhang Y, Zhou J, Jin Y, Liu C, Zhou H, Sun Y, *et al*. 2024. Single-cell and bulk transcriptomics reveal the immunosenescence signature for prognosis and immunotherapy in lung cancer. Cancers (Basel). 17(1):85.